In-beam aerogel light yield characterization for the AMS RICH detector

M. Aguilar-Benitez[a], L. Arruda[b], F. Barao[b,*], G. Barreira[b], A. Barrau[c], B. Baret[c], J. Berdugo[a], M. Buénerd[c], J. Casaus[a], I. Cernuda[a], D. Crespo[a], C. de la Guia[a], C. Delgado[a], C. Diaz[a], L. Derome[c], F. Giovacchini[a], P. Goncalves[b], A. Keating[b,1], G. Laurenti[d], A. Malinine[c], C. Mañá[a], J. Marín[a], G. Martinez[a], A. Menchaca-Rocha[f], R. Pereira[b], M. Pimenta[b], E.-S. Seo[e], M. Vargas-Trevino[c]

[a] CIEMAT, Avenida Complutense 22, E- 28040 Madrid, Spain
[b] LIP, Avenida Elías García 14- 1, P- 1000 Lisboa, Portugal
[c] LPSC, IN2P3/CNRS, 53 av. des Martyrs, 38026 Grenoble cedex, France
[d] University of Bologna and INFN, Via Irnerio 46, I- 40126 Bologna, Italy
[e] University of Maryland, College Park, MD 20742, USA
[f] Instituto de Física, UNAM, AP 20- 364 Mexico DF, Mexico

[*] Corresponding author.
[1] Present address: CERN, Geneva, Switzerland.

Abstract

The ring imaging Cherenkov (RICH) detector of the AMS-02 spectrometer provides a very precise measurement of the electric charge and velocity. The RICH detector is composed of a conical reflector ended on top by a dual radiator plane made of sodium fluoride and aerogel, and at the bottom by a detector plane made of pixelized photomultipliers. The vast majority of the events ($\sim$ 90%) that are collected in the RICH cross the aerogel radiator. Therefore, the choice and characterization of the aerogel radiator is essential for reaching the design goals. A prototype of the RICH detector was built for both concept proof and testing of the different elements. Beam tests with the RICH prototype and using several aerogel radiator samples were performed at CERN in 2002 and 2003. This note summarizes the method used and the results obtained for the light yield of different aerogel samples.

Keywords: AMS; RICH; Space instrumentation; Cherenkov imaging; Charged particle detectors; Aerogel; Aerogel light yield

1 Introduction

The AMS spectrometer stands at the forefront of the new generation of instruments for space experiments. It is a large acceptance ($0.5 \mathrm{m}^2 \mathrm{sr}$) detector based on a superconducting magnet designed for long-duration operation in space. It will be installed on the International Space Station for a long-term experimental campaign of three or more years. The main purposes of the experiment are the search for primordial antimatter and for dark matter in space [1]. In addition, the instrumental capabilities of the experiment for momentum measurement and particle identification required for these studies also open highly promising prospects for other astrophysics and astroparticle physics studies involving cosmic ray detection, from γ to nuclear particles. The instrumental architecture of the AMS spectrometer is described elsewhere [1, 2].

The RICH [3] detector of AMS plays a major role in event reconstruction, providing very precise measurements of particle velocity and charge. It is composed, from top to bottom, of the following components (Fig. 1):

- a radiator plane made of aerogel ($n = 1.05$) tiles with a thickness of 2.5cm and sodium fluoride crystals ($n = 1.334$) in the central region, 0.5cm thick;
- a conical reflector surrounding the $\sim$ 47cm high expansion volume;
- a detection plane made of 680 multipixelized Hamamatsu photomultipliers (R7600-M16) coupled to solid plastic light guides with a pixel size of 8.5mm;
- individual magnetic shieldings on photomultipliers to deal with the large stray field.

In the AMS RICH detector, the velocity and charge of crossing particles are determined from the Cherenkov photons ring reconstruction. From event to event, different photon patterns can be obtained depending on particle velocity, impact point and direction. The determination of the radiated photons' aperture angle (θ_c), after the pattern reconstruction, allows to derive the particle's velocity, $\beta = 1/n \cos\theta_c$. On the other hand, the particle's charge derives from the signal associated with the photon ring (N_{pr}), according to $Z^2 \propto (N_{pr}/\epsilon) 1/\sin^2\theta_c$ where ϵ is an overall efficiency factor that includes both the ring acceptance and the photon detection efficiency (absorption and scattering effects included).

Apart from the Cherenkov ring, charged particles also produce a signal in the region where they pass the detection matrix, due to the acrylic light guide crossing. This signal is concentrated in a few pixels and is much stronger than the one from ring hits. It is not considered for ring reconstruction.

The AMS goals on mass separation for light isotope identification up to beryllium and charge separation up to iron ($Z = 26$) impose severe constraints on the RICH design and monitoring. A velocity accuracy of 10^{-3} for singly charged particles is aimed. At least three hits in the Cherenkov ring are necessary for a reliable event reconstruction due to the presence of noisy hits from aerogel scattered photons or photomultiplier dark current. The more hits (and photoelectrons) are present in the ring the better is the accuracy of the velocity measurement as stated by the following expression:

$$\frac{\Delta\beta}{\beta} = \frac{\tan\theta_c \Delta\theta_c}{Z\sqrt{N_{Z-1}}} \tag{1}$$

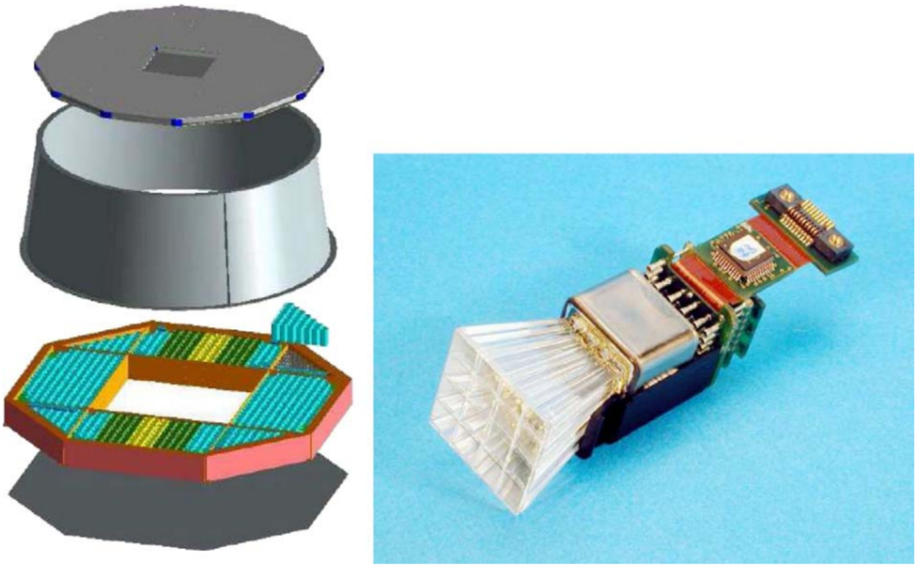

Figure 1: (Left) Exploded view of the AMS-02 RICH detector. From top to bottom the radiator plane, the conical reflector and the detection plane. (Right) Individual detection cell including the light guide, the photomultiplier, the cell housing and the front-end electronics.

where θ_c is the Cherenkov angle and N_{Z-1} is the number of photoelectrons observed for $Z = 1$ particles. The single hit Cherenkov angle uncertainty ($\Delta\theta_c$) depends on the detector pixel size and radiator's thickness and chromaticity.

The quality of charge measurement depends on the number of Cherenkov photons detected. Uncertainties on individual charge measurements arise from statistical fluctuations on the collected signal and photomultiplier amplification ($\sigma_{pe} \sim 0.5 - 0.6$) and systematic effects from variations on radiator tiles (thickness, optical properties), mirror reflectivity and readout matrix (photomultiplier gain, detection cell efficiency):

$$\Delta Z = \frac{1}{2}\sqrt{\frac{1+\sigma_{pe}^2}{N_{Z-1}} + Z^2\left(\frac{\Delta N}{N}\right)^2_{syst}}. \quad (2)$$

The statistical uncertainty, dominant in the low charge region, does not depend on the charge as the Cherenkov signal increases with Z^2. On the other hand, it depends on the number of photoelectrons (N_{Z-1}) expected for singly charged particles. Systematic errors in light yield estimation become dominant at high charges and have to be limited in order to fulfill the requirement of charge separation up to iron [4]. For instance, requiring a charge error (ΔZ) lower than 0.3 charge units as a criterion for charge separation on iron region and assuming a statistical error ~ 0.2 (corresponds to $N_{Z-1} \sim 8$), an upper limit for the systematic uncertainty of $\sim 1.5\%$ is obtained.

Therefore, the higher is the aerogel light yield the better will be the uncertainty on the velocity and charge determination. In addition, the reconstruction efficiency increases with light yield. The present note summarizes the procedure and results of the light yield characterization studies based on the results of the in-beam tests performed at CERN in 2002 and 2003 using a prototype of the AMS RICH [5].

2 RICH prototype tests

The research effort leading to the final AMS-02 RICH detector included the construction of a RICH prototype which underwent cosmic-ray testing at LPSC in Grenoble and two in-beam tests at CERN. The prototype, shown in Fig. 2, corresponds to a fraction of the final detector. It included a detection matrix with 96 Hamamatsu R7600-M16 photomultipliers, each with 4×4 pixels, coupled to solid light guides.

Figure 2: The AMS RICH prototype.

The first prototype test was performed in mid-2002 at LPSC by exposing the detector to the cosmic-ray flux at ground level. Later, in-beam testing took place at CERN SPS in October 2002 and October 2003 using secondary beams of nuclear fragments. The momentum resolution of the beam line was set to 1%, similar to the expected uncertainty in the AMS apparatus [6]. The 2002 beam was produced by bombarding a beryllium (Be) target with 20GeV/c nucleon lead (Pb) ions, while the 2003 beam was obtained from the bombardment of a lead target with indium (In) ions having a momentum of 158GeV/c nucleon. These primary beams used on both years allow to test the detector over a large range of charges. A selection of certain fragmented isotopes or charges can be performed through A/Z beam settings. The values of $A/Z = 2, 2.25, 2.35$ were used. During parts of the 2003 test the experimental set-up was completed with a mirror segment corresponding to a 30-sector (1/12 of total). Other subdetector parts of the AMS spectrometer were also present during the CERN tests [7, 8]. The full apparatus is shown in Fig. 3.

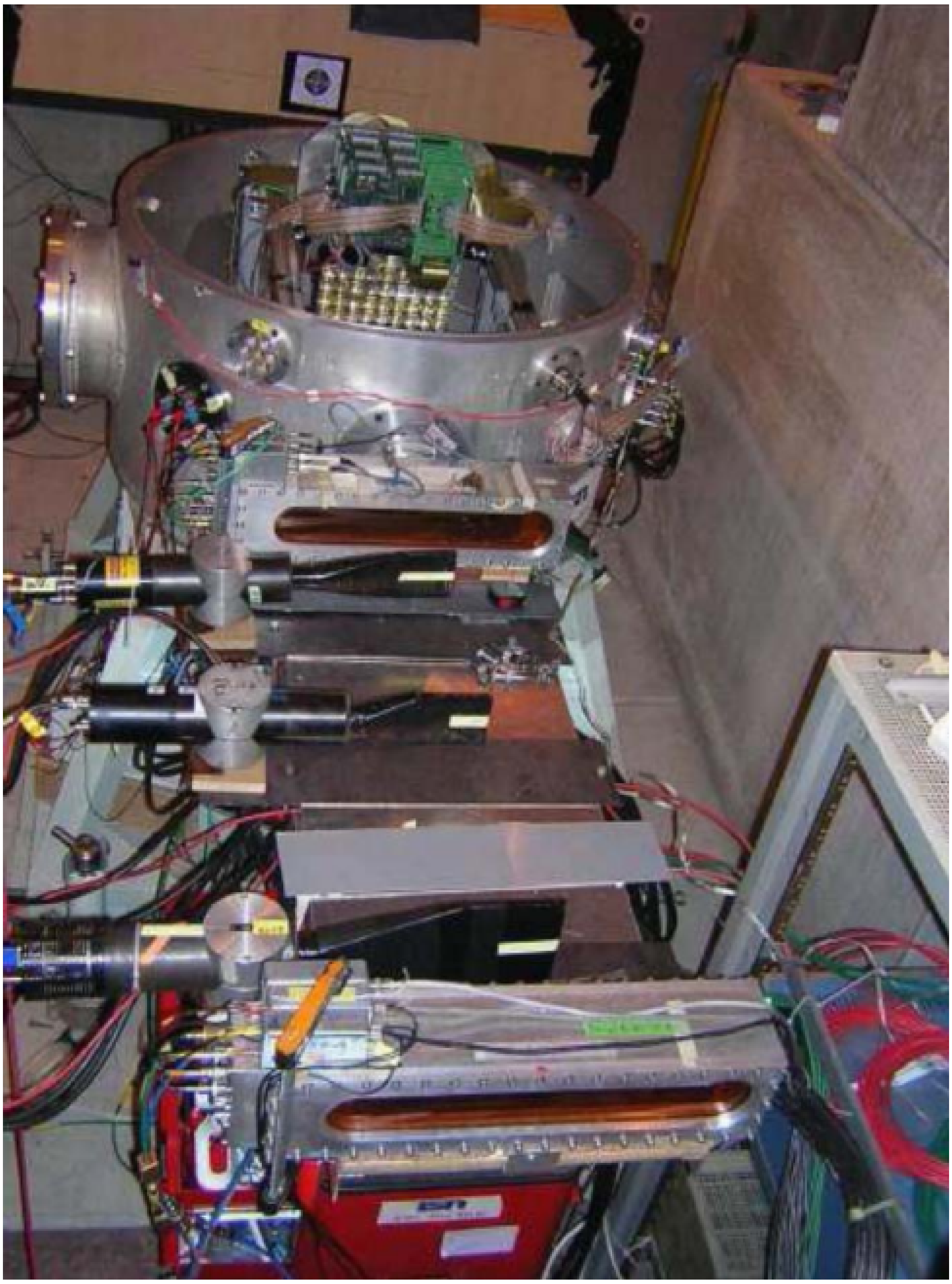

Figure 3: Experimental set-up for the 2003 beam test at CERN. The RICH prototype is at the top of the image.

A total of seven aerogel samples from two manufacturers were tested at different beam energies during the 2002 and 2003 campaigns.

In the 2002 beam test five aerogel samples were tested. Three of them from Matsushita Electric Works (MEC) [9] with refractive indices 1.03 (two samples) and 1.05, and other two from the Boreskov Institute of Catalysis in Novosibirsk (CIN) [10] with refractive indices 1.03 and 1.04. The test beams used were composed of secondary protons produced by coalescence and having momenta of 5, 7, 9, 11 and 13GeV/c.

In the case of the 2003 test, helium beam fragments with 158GeV/c/nucleon were used. Three aerogel samples were tested, one of which (CINy02.103) had already been used in the 2002 test. The other two samples had a refractive index 1.03 from Matsushita and a refractive index 1.05 from the Boreskov Institute. Table 1 summarizes the samples and beam conditions used in 2002 and 2003.

The design of the radiator plane includes a 0.75mm methacrylate foil in front of the radiator titles. One of the aerogel samples was tested including a polyester foil which was worst in optical properties than the one to be used in the final detector.

The analysed samples in 2002 had a number of events ranging from $\sim 1 \times 10^4$ to $\sim 5 \times 10^4$ while the samples in 2003 had $\sim 10^5$ events each.

Table 1: Aerogel samples used in the beam tests.

Year	Sample	Refractive index	Thickness (mm)	Foil	Beam conditions
2002	MECy02.103	1.03	2×11	No	Protons, 5-13 GeV/c
	MECy02.105	1.05	2×11	No	Protons, 7-13 GeV/c
	MECy01.103	1.03	3×11	Yes	Protons, 5-13 GeV/c
	CINy02.104	1.04	30	No	Protons, 5-13 GeV/c
	CINy02.103	1.03	30	No	Protons, 5-13 GeV/c
2003	CINy02.103	1.03	30	No	He, 158 GeV/c/nucleon
	MECy03.103	1.03	3×11	No	He, 158 GeV/c/nucleon
	CINy03.105	1.05	25	No	He, 158 GeV/c/nucleon

3 Data selection

Among the data collected in 2002 and 2003 test beams, a large number of events correspond to particles crossing the prototype detector in a perpendicular way. Such events will generate a circular Cherenkov ring in the detector matrix.

In the 2002 analysis, two kinds of background events were identified and had to be rejected from the data samples. Firstly, a significant muon contamination was present in particular at low momenta. These events, having a different velocity from protons, will have a larger Cherenkov ring signal. In addition, a significant fraction of events present a large number of noisy hits when compared to the expected number arising from the aerogel scattering. Such noisy hits can contribute to a systematic shift in the evaluated Cherenkov ring signal. Fig. 4 displays proton (clean and noisy) and muon events collected in the 2002 test.

The fact that protons and muons have different masses allows to use the velocity measurement as a discriminant observable for muon rejection. Fig. 5 shows the reconstructed velocity distributions for radiator MECy02.103 at beam momenta of 5, 7, 9, 11 and 13GeV/ c. For lower momenta the muon peak is clearly seen at $\beta \simeq 1$, while protons peak near but not exactly at the expected velocity. The observed proton peak in

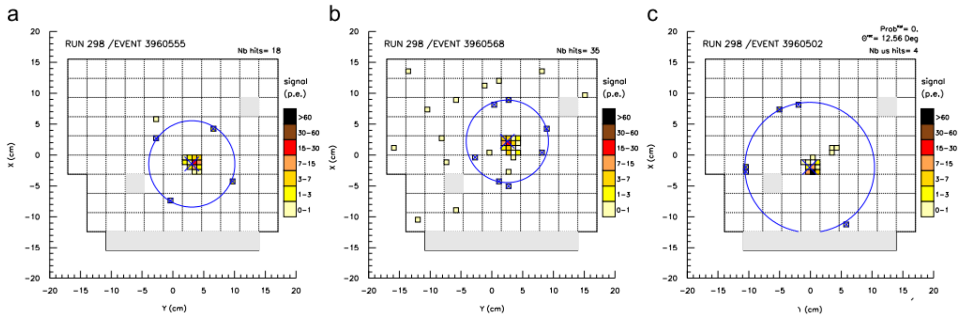

Figure 4: Event displays of reconstructed rings for protons (a,b) and muons (c) of $p = 5\text{GeV}/c$; the proton event reconstructed in (b) contains a large number of noisy hits.

the velocity distribution was used to obtain a corrected value for the beam momentum. To exclude muon events, and moreover bad reconstructions of proton events, only reconstructed velocities within $3\sigma(\beta_{\text{peak}} \pm 0.003)$ were considered. The larger the beam energy was the smaller the muon component became, vanishing at higher energies.

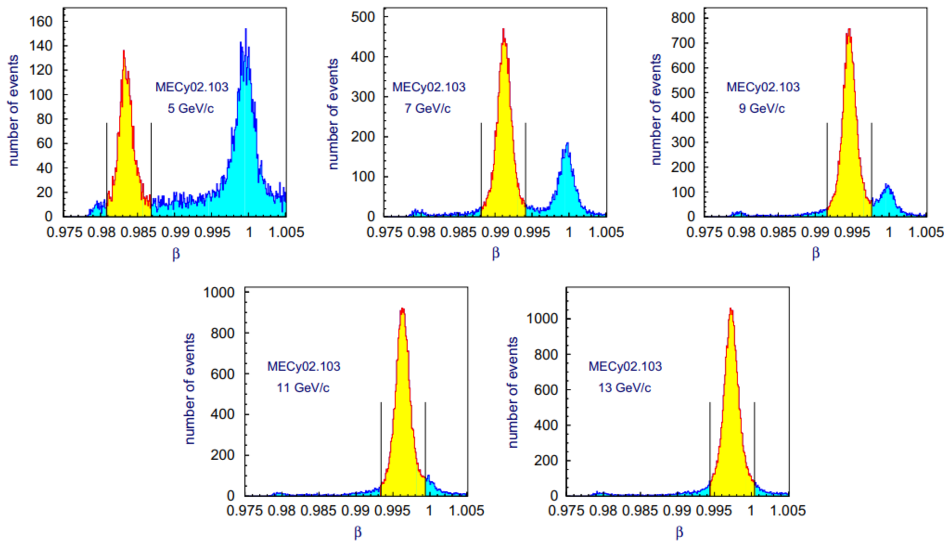

Figure 5: Distributions of reconstructed velocity using the same radiator at different momenta. Vertical lines show the acceptable velocity range. Muon contamination, which is stronger at low momenta, appears as an additional peak at $\beta = 1$.

The accurate measurement of average proton velocity for each run, obtained from the RICH prototype showed small differences with respect to the expected value. The RICH measurements were used to obtain a better estimate of particle momentum.

The events with noisy hits were addressed by studying the correlation between the number of hits inside and outside the Cherenkov ring. In normal conditions, the number of hits associated with the ring signal and the number of noisy hits should be uncorrelated. Fig. 6(a) shows, for a data sample from a 5GeV/c proton beam impinging on aerogel MECy02.103, a strong correlation above a number of noisy hits around 5. Although the fraction of noisy events is significantly smaller at higher energies, similar correlations were found for all the other test energies and aerogel samples. Therefore, a clear bias in the measured ring signal is observed. To reduce this effect in the data samples, a cut on the number of noisy hits in the event was applied. Only events with a number of noisy hits lower than 5 were selected. Fig. 6(b) shows the distribution of all the hits in the detection matrix in terms of its active inner area, for a 5GeV/c proton sample. After applying the noisy hits cut, the signal in the Cherenkov ring to background ratio is strongly improved. Fig. 6(c) shows the effect on the data sample applying both the velocity and noisy hits cut.

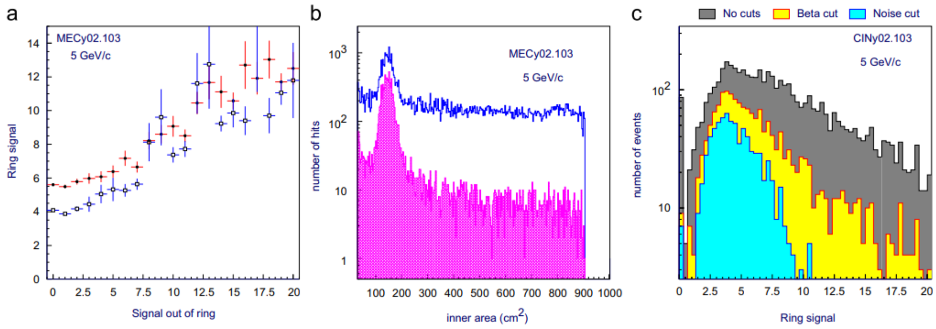

Figure 6: Data sample of 5GeV/c protons. (a) Average Cherenkov ring signal as function of non-ring signal before (full dots) and after (open squares) applying the velocity cut. (b) Signal distribution as function of its active inner area before and after applying the noisy hits cut. The rise to the left of the peak corresponds to the tail of the charged particle signal. (c) Cherenkov ring signal distribution after applying the different cuts.

4 Light yield determination

An evaluation of the signal associated with the Cherenkov rings needs to be performed in order to determine the aerogel light yield. The reconstruction of the Cherenkov rings was performed using an algorithm developed for the full-scale RICH detector [11] and adapted to the prototype set-up. This approach uses a maximum likelihood method based on the calculation of distances between individual hits and the Cherenkov ring. The estimated Cherenkov angle corresponds to the maximum probability of having the detected hits belonging to the ring. The ring signal is obtained by adding the signal of the hits within a ring distance of 1.3cm.

In general, during both 2002 and 2003 tests, the Cherenkov rings produced by beam particles were not fully contained in the PMT matrix. Additionally, small regions of dead pixels were observed in the readout matrix as shown in Fig. 7(a). Therefore, the evaluation of the aerogel photon yield implies the knowledge of the visible fraction of the Cherenkov ring (ring acceptance). The procedure for the ring acceptance estimation is described in Ref. [12] for null-width rings. In this note, the effect of the ring width was taken into account. Sampling the ring acceptances at five different Cherenkov angles around the fitted value, $\theta_c = \theta_c^0 + i\sigma_{\theta_c}$ with $i = 0, \pm1, \pm2$, the mean ring acceptance can be calculated according to $\epsilon = \sum_i \epsilon_i w_i / \sum_i w_i$. Assuming a Gaussian distribution, the weight factor is given by $w_i = e^{-i^2/2}$. Figs. 7(b) and (c) present the evaluated ring acceptances for two data samples with $p = 13$GeV/c nucleon and aerogel refractive indices $n = 1.03$ and 1.05. Acceptances lower than 1 observed in the case of the 1.03 aerogel data sample are essentially due to dead areas in the PMT matrix, while in addition the acceptance for the 1.05 aerogel reflects the larger Cherenkov rings which in many cases are not fully contained within the detection matrix.

The signal distribution associated with a given aerogel data sample will depend on:

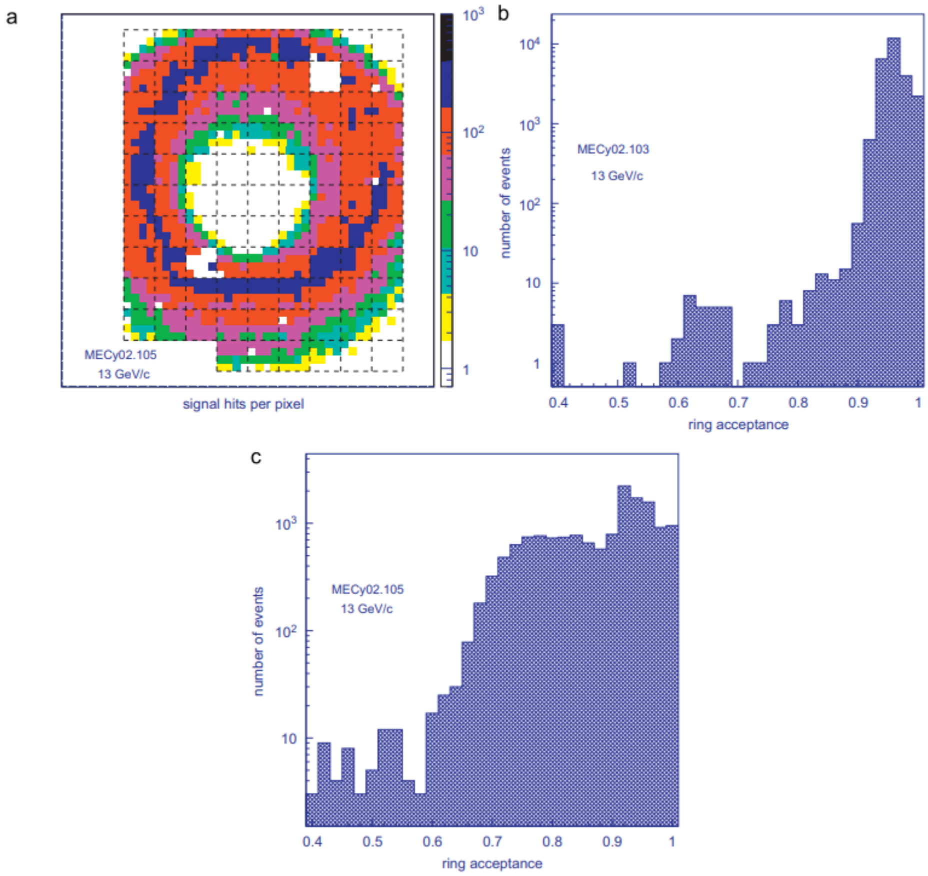

Figure 7: (a) Distribution of the number of ring hits detected in each pixel for a single data sample at 13GeV/c (b,c) Ring acceptance distributions at 13GeV/c for two radiators in the 2002 beam test.

- Ring acceptance: For events having a ring acceptance ϵ, the mean number of photoelectrons expected (N) will be given according to $N = \epsilon N_0$, where N_0 is the expected number of photoelectrons in a fully contained ring.

- Statistical fluctuation: Moreover, the observed number of hits (i) for a sample with a given acceptance ϵ and a mean number of photoelectrons N, will fluctuate according to a Poisson law $p(i) = e^{-N} N^i / i!$.

- Photomultiplier gain: Finally, the detected signal in the photomultiplier anode is related to the number of photoelectrons generated in the photocathode, by a gain factor of the order of 10^6. This results from the photoelectron amplification along the dynode chain. The statistical nature of the amplification process induces an uncertainty in the gain of the order of $0.5 - 0.6$ photoelectrons. The signal distributions for $i = 1$ and $i = 3 - 6$ photoelectrons, reflecting the uncertainty in the chain amplification, are shown, respectively, in Figs. 8(a) and (b).

In the 2002 analysis, the radiator tiles were studied using proton beams with a relatively large spread ($\sim$ 2cm). This implies a large variation in the ring acceptance. In addition, a low number of photoelectrons was expected. Therefore, the distribution of detected ring signals, x, may be parameterized as a function of the expected number of photoelectrons in a fully contained ring (N_0) and a normalization factor A corresponding to the total number of events being analysed,

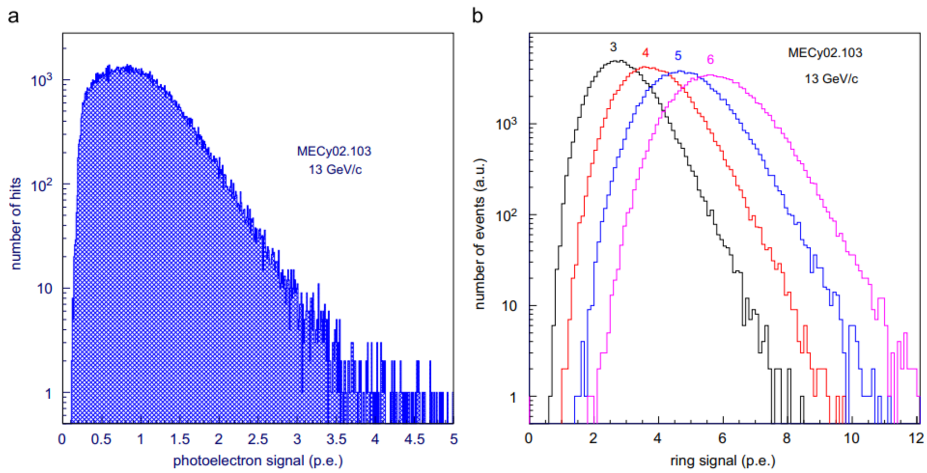

Figure 8: (a) Hit signal distribution for a high momentum sample. (b) Expected signal distribution for sets of 3-6 photoelectrons in this sample.

$$f(x; N_0, A) \propto \sum_{i=1}^{\infty} \sum_{i=1}^{N} P(\epsilon_i) \frac{e^{-x}(\epsilon_i N_0)^i}{i!} f_i(x) \qquad (3)$$

where $P(\epsilon_i)$ is the fraction of events with geometrical acceptance ϵ_i and $f_i(x)$ corresponds to the signal distribution for i hits. The ring signal distributions and corresponding fits for three different samples corresponding to different aerogel radiators and energies, are shown in Fig. 9.

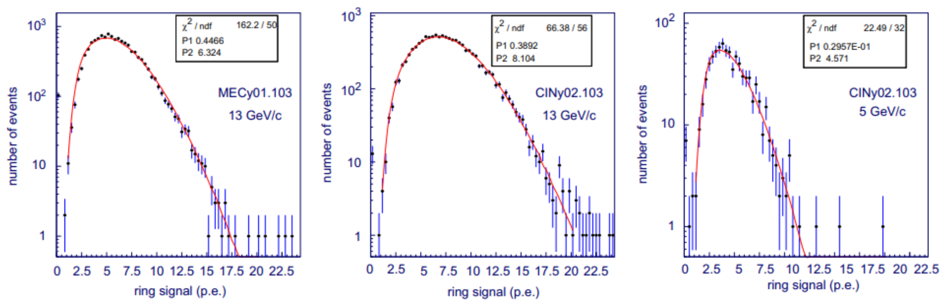

Figure 9: Fit to reconstructed signal distribution for three data samples.

In the case of the 2003 test, the aerogel tiles were studied with a selection of helium ($Z = 2$) events of 158GeV/c nucleon. Comparing to 2002, the particle beam was narrower ($\sim$ 1mm) and therefore the Cherenkov rings had a constant ring geometrical acceptance. Moreover, the usage of helium events implied a larger number of ring photoelectrons expected by a factor 4 and following a Gaussian law. In this context, the calculation of the light yield corresponding to a fully contained ring was simplified. A Gaussian fit was applied to the signal distribution (Fig. 10) and the result obtained was divided by the ring acceptance.

In 2002, the presence of beams with different energies allowed to check the consistency of the different measurements. In addition, it can be used to derive the expected light yield at $\beta = 1$, for each aerogel sample. This can be attained by fitting the set of results obtained for a given radiator at different energies to the expression giving the evolution of the light yield ($N_{\rm pe}$) with particle momentum:

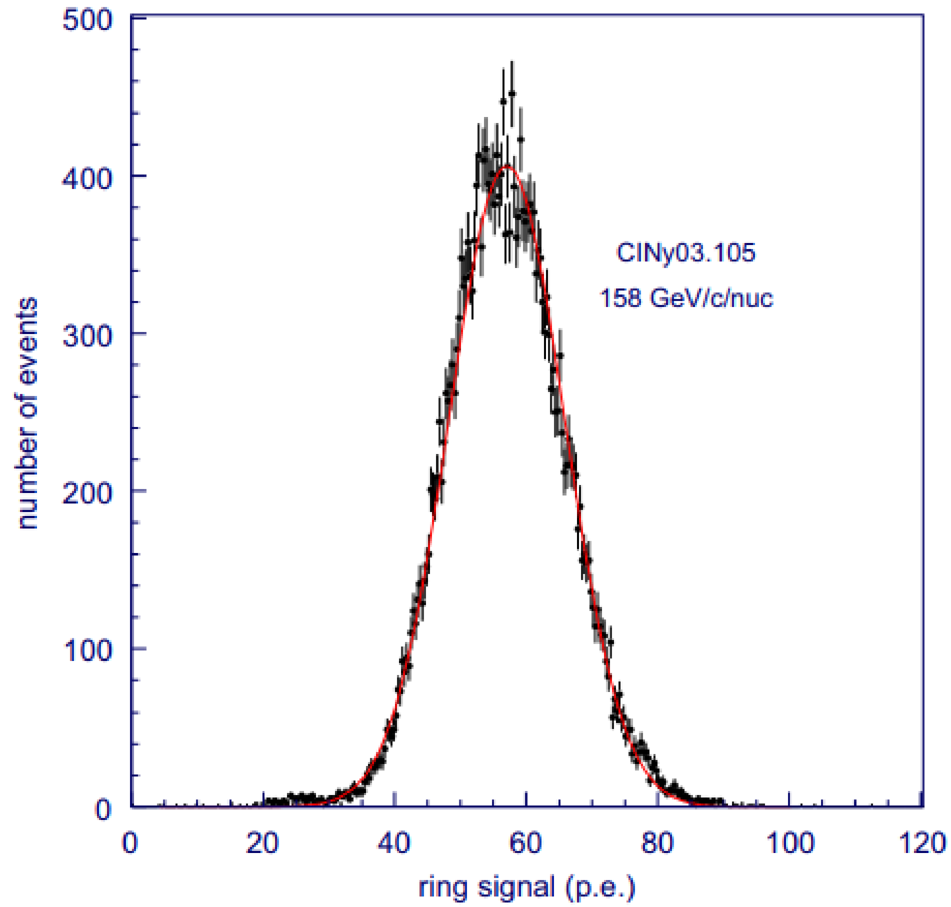

Figure 10: Reconstructed signal distribution of helium events in 2003 test (CINy03.105, 158 GeV/c).

$$N_{\rm pe} = N_0^{\beta=1}\left[1 - \frac{(m/p)^2}{n^2-1}\right] \quad (1) \tag{4}$$

where $N_0^{\beta=1}$ is proportional to $(n^2-1)/n^2$ and depends linearly on the sample's thickness and radiator absorption.

5 Systematic corrections and uncertainties

Several factors related to signal threshold and calibration, and background from noisy hits can affect the light yield estimates. In addition, the presence of a radiator plastic foil in some of the runs lead to a reduced light yield. A full description of these effects and their implication on the 2002 and 2003 data analysis is reported in the following paragraphs.

5.1 Pixel noise

Despite the applied selection criteria, a significant fraction of noisy hits remained on the 2002 data samples. The signal associated with the collected hits, regardless of the proton beam energy, should reproduce the photoelectron distribution. The existence of a possible contamination on the different samples was checked. A background component, identified as an excess of low-signal hits, was observed in the lower momenta beam samples. Fig. 11 shows the hits signal distributions for different 5GeV/c samples. The excess of low-signal hits is clearly visible in distributions (b) and (c).

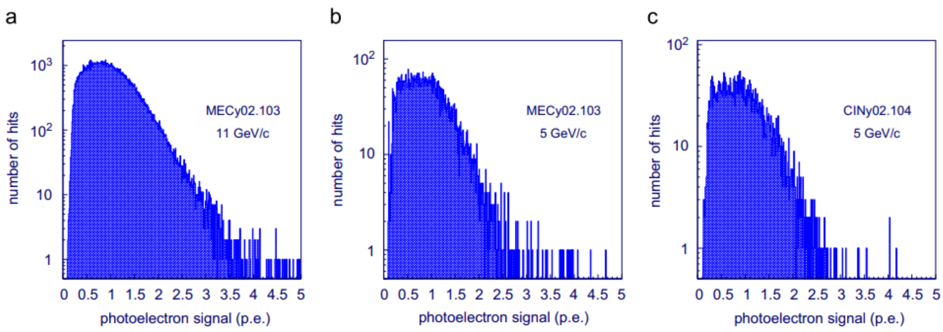

Figure 11: Distribution of hit signals for three data samples.

The effect of the noisy hits in the light yield evaluation may be estimated assuming that in each sample the observed ring signal S is the sum of a true signal S and a background contribution S_{B}. The magnitude of the signal correction is given by the following expression:

$$\frac{\langle S \rangle}{\langle S \rangle} = \frac{N_{\mathrm{B}} \langle S_{\mathrm{B}} \rangle}{N} \frac{N}{N} = \frac{N}{N} \tag{5}$$

where $N = N + N_{\mathrm{B}}$ is the observed number of ring hits, N is the number of signal hits and N_{B} is the number of background hits. For each sample a comparison of the photoelectron profile, obtained at higher momentum (13GeV/c), with the observed hit signal profile is performed. Assuming that contamination is only present in hit signals below 0.6 p.e., the fraction of background hits N_{B}/N and the average signal of background hits $\langle S_{\mathrm{B}} \rangle / N_{\mathrm{B}}$ can be derived. The estimated fraction of background hits was lower than $\sim 3\%$ for beam momenta of 7GeV/c or higher while for the 5GeV/c samples, a more significant noise correction, at the level of $\sim 5 - 10\%$ was derived.

5.2 Signal threshold

To reduce the RICH event size a minimal hit signal (threshold) is applied to the gathered pixel signals. Only ADC counts clearly above the pedestal ($4\sigma_{ped} \sim 15$) are collected. The presence of this threshold may introduce a bias in the ring signal estimate since very low signal hits may remain undetected. On the other hand, PMT noise if above threshold can contribute with additional hits to the ring signal.

This signal threshold effect was evaluated by performing simulations switching on and off thresholds, for each individual data sample. Simulation results showed that such effect was negligible in the 2003 test but significant in the 2002 test where a fraction up to 8% of hits was not detected. The corresponding reduction in the total ring signal was not as significant since these non-detected hits have very low signals.

5.3 Sample calibration

In the 2002 analysis, the photoelectron calibration is automatically taken into account on the light yield method by the inclusion of the photoelectron signal profile in the fitting procedure.

In the case of the 2003 analysis such calibration is not feasible since the Cherenkov patterns studied corresponded to events with $Z = 2$ where a significant fraction of ring hits correspond to the detection of more than one photon. It was observed that the average signal of scattered hits, where the effect of double photons should be negligible, showed significant deviations from 1, fluctuating between runs. Such fluctuations, which cannot be estimated for ring hits, have a direct effect on the light yield evaluation and were considered as a systematic error with a magnitude of 3%.

In addition to the sample calibration, the dispersion of individual PMT gains was checked. A large statistics of hits per PMT was collected in order to ensure a good accuracy of the gain evaluations. Some non-uniformities were observed, with a spread $\sigma_{PMT} \sim 5\%$ in distribution of the average PMT signals. Fig. 12 shows the variation of the average signal between PMTs. Since in each sample the Cherenkov rings cover an area of ~ 20 PMTs, the estimated systematic error on the photoelectron calibration is $\sigma_{cal} \sim \frac{5\%}{\sqrt{20}} \simeq 1\%$.

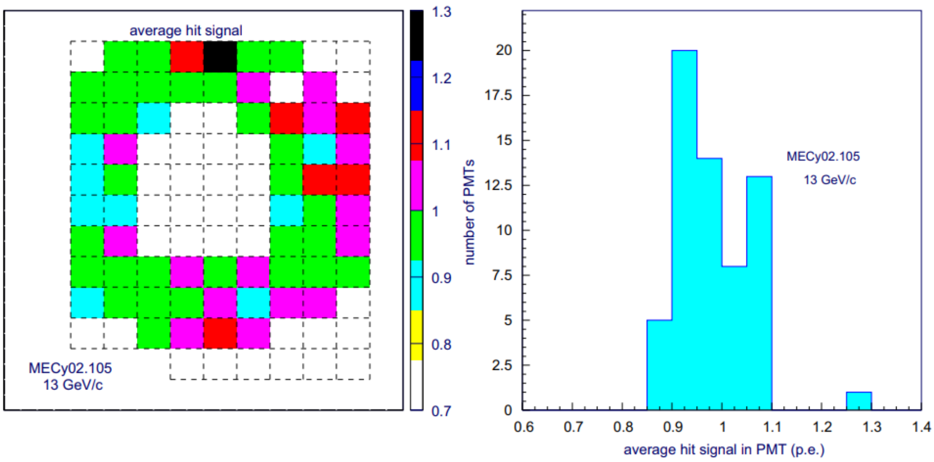

Figure 12: Average photoelectron signal in different PMTs as fraction of global average for a data sample: results by PMT (left), overall distribution (right). PMTs shown in white did not have significant statistics and were not included in the overall distribution.

5.4 Foil attenuation

In the case of radiator MECy02.103 an additional correction had to be estimated since this was the only radiator for which a polyester foil was used. This polyester foil absorbed a significant fraction of the light produced in the aerogel. Simulations were used to estimate photon absorption, giving a light yield reduction of 17%.

6 Light yield results

The procedures and corrections described in the previous sections were applied to obtain light yield estimates for the aerogel samples tested in 2002 and 2003. Table 2 presents the mean light yield results obtained for full acceptance rings and for the different aerogel samples tested in 2002 and 2003.

The evolution of the light yield for the aerogel samples tested in 2002 as function of the beam proton momentum is shown in Fig. 13. The fit to the experimental values

Table 2: Event data samples and corresponding light yield estimates.

Year	Sample	Beam momentum (GeV/c)	Light yield estimate (p.e.)
2002	MECy02.103	5	5.085 ± 0.002
	MECy02.103	7	7.050 ± 0.006
	MECy02.103	9	9.036 ± 0.013
	MECy02.103	11	10.945 ± 0.023
	MECy02.103	13	12.741 ± 0.036
	MECy02.105	7	7.012 ± 0.006
	MECy02.105	9	8.933 ± 0.012
	MECy02.105	13	12.526 ± 0.034
	CINy02.103	5	5.099 ± 0.002
	CINy02.103	9	9.224 ± 0.014
	CINy02.103	13	13.681 ± 0.044
	MECy01.103	5	5.237 ± 0.003
	MECy01.103	7	7.258 ± 0.007
	MECy01.103	9	9.307 ± 0.014
	MECy01.103	13	13.161 ± 0.039
	CINy02.104	5	5.323 ± 0.003
	CINy02.104	7	7.204 ± 0.007
	CINy02.104	9	8.980 ± 0.013
	CINy02.104	13	11.881 ± 0.029
2003	CINy02.103	158	10.53 ± 0.37
	MECy03.103	158	11.04 ± 0.39
	CINy03.105	158	14.59 ± 0.51

performed using expression (1) shows a good agreement with light yield measurements for the different aerogel samples. The light yields for full acceptance rings and normalized to $\beta = 1$, $N_0^{\beta=1}$ are derived from the fits.

Table 3 summarizes the light yield results obtained for full acceptance rings and normalized to $\beta = 1$, for all aerogel samples tested in 2002 and 2003. Results for radiator MECy01.103 have been corrected to take the presence of a foil into account. One of the samples used in 2003, CINy03.105, had the highest light yield by a large margin despite having a relatively low thickness (25 mm).

The decision regarding the radiator to be used in the final detector required a comparison of the light yield of different aerogel samples normalized to a common thickness. The reference value for thickness was chosen to be 25 mm. Simulations were performed for each sample (except those that had a thickness of exactly 25 mm) using the real and reference thicknesses. A correction factor was derived and used to rescale the light yield values to the reference thickness.

Fig. 14 shows the rescaled light yield results for all aerogel samples. One sample, CINy03.105, had the highest light yield by a wide margin. The material of this sample was chosen to integrate the final radiator of the AMS-02 RICH detector.

Results obtained for the light yield at different energies with the same aerogel sample may be used to obtain an estimate of its refractive index. This is done by performing a fit to expression (1) with two free parameters, n and $N_0^{\beta=1}$. Table 4 summarizes the results obtained applying this fit to the results of the 2002 test (Fig. 15). The reference values of

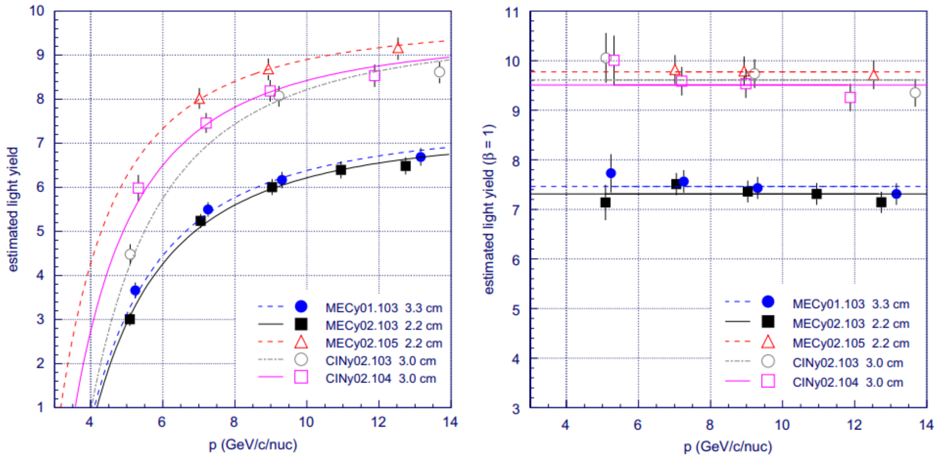

Figure 13: Evolution of light yield with particle momentum for the different aerogel samples tested in 2002. Points correspond to results obtained for each sample, while lines are the result of a fit to the available points for each aerogel sample. The left-hand plot shows the average number of photoelectrons for a fully contained ring at each momentum, while the right-hand plot has all values rescaled to the $\beta = 1$ case.

Table 3: Light yield estimates $\beta = 1$ for aerogel samples.

Sample	$N_\beta^{(\beta=1)}$ (p.e.)
2002:	
MECy01.103	9.00 ± 0.15
MECy02.105	9.78 ± 0.17
CINy02.103	9.61 ± 0.19
MECy02.103	7.31 ± 0.10
CINy02.104	9.51 ± 0.16
2003:	
CINy02.103	10.53 ± 0.37
MECy03.103	11.04 ± 0.39
CINy03.105	14.59 ± 0.51

n, obtained from previous estimation [13], are shown for comparison. A good agreement is observed.

7 Prospects for AMS-02

The results presented in this note for the selected aerogel sample (CINy03.105) may be used to estimate the average number of photons which should be detected in AMS-02 events. However, such extrapolation must take into account several differences, presented in Table 5, that exist between the prototype and flight configurations.

The detection matrix used in the prototype corresponds to a fraction (96 PMTs) of the final AMS-02 RICH detector (680 PMTs). While the PMTs used in both configurations are identical, the spacing between them was increased in the flight configuration to make room for placing a magnetic shielding around each PMT. The pitch increased from 31mm

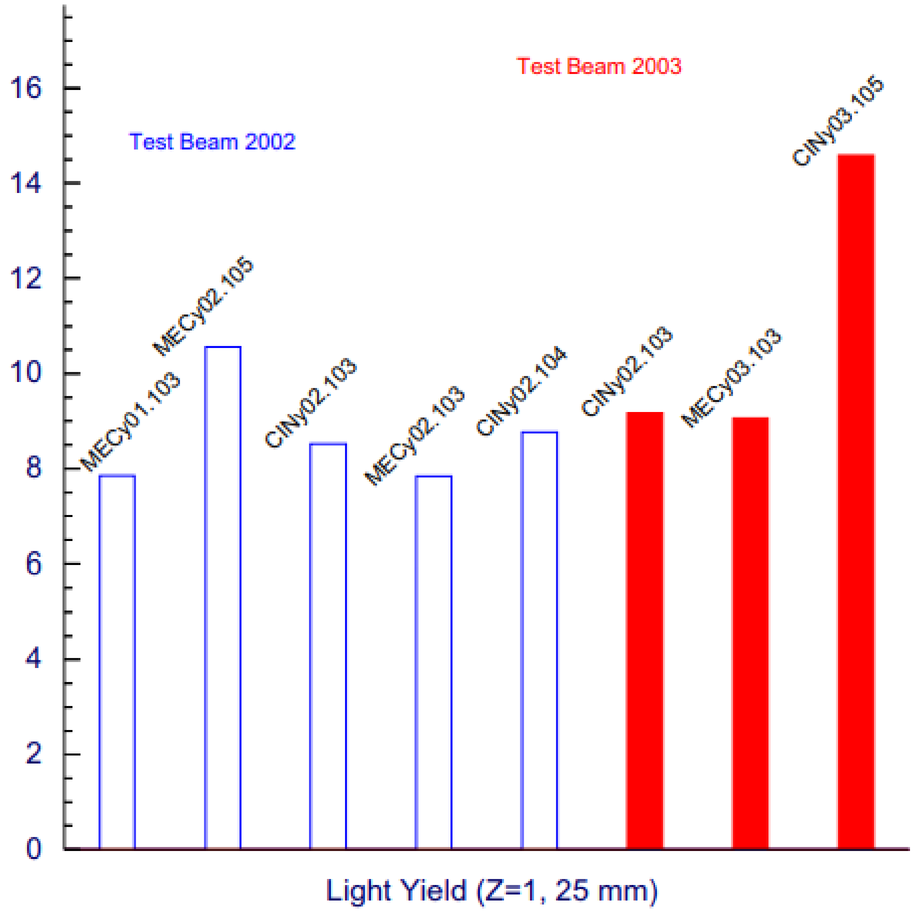

Figure 14: Comparison of aerogel light yields rescaled for a thickness of 25mm

in the prototype to 37mm in the flight configuration. The side of the light guides top surfaces was increased from 31mm to 34mm, meaning a pixel size increase from 7.75 to 8.5mm. In addition, the dead spaces between neighbouring photomultipliers, which were negligible in the prototype, became significant in the flight matrix, corresponding in average to 15.6% of the detection surface area.

Not only the light guide geometry has changed, but also the materials used. Increased transparency was obtained by replacing the acrylic plastic from Saint-Gobain (Bicron BC-800) used in the prototype with another acrylic plastic, Diakon LG-703, from Lucite International. The transparent foil glued to the light guide pipes was also changed, from Bicron BC-800 in the prototype to Hesaglas, from the Peerless company, in the flight configuration. The light guide response was studied by simulating photons according to the radiation Cherenkov spectrum folded with the photomultiplier quantum efficiency and radiator absorption. Fig. 16(a) shows the light guide efficiency for the prototype and flight models as function of the incidence photon angle, measured with respect to the light guide axis. The light guides used in the flight configuration are more efficient for light collection at low incidence angles. The photon incidence angles on the top of the light guide, imposing the trigger conditions expected on the flight configuration of the AMS detector, range from 0 to 50. On the other hand, the usage of a perpendicular beam in the data runs implies a fixed value on the photon incidence angle. Fig. 16(b) shows the distribution of the photon incidence angle on top of the light guide for the prototype and

Table 4: Light yield results leaving n as a free parameter.

Sample	$N_\beta^{(\beta=1)}$ (p.e.)	n (fit)	n (reference)
MECy01.103	8.83 ± 0.22	1.0319 ± 0.0027	1.03
MECy02.105	9.71 ± 0.38	1.0505 ± 0.0156	1.05
CINy02.103	9.44 ± 0.24	1.0319 ± 0.0025	1.03
MECy02.103	7.32 ± 0.14	1.0289 ± 0.0017	1.03
CINy02.104	9.25 ± 0.26	1.0432 ± 0.0062	1.04

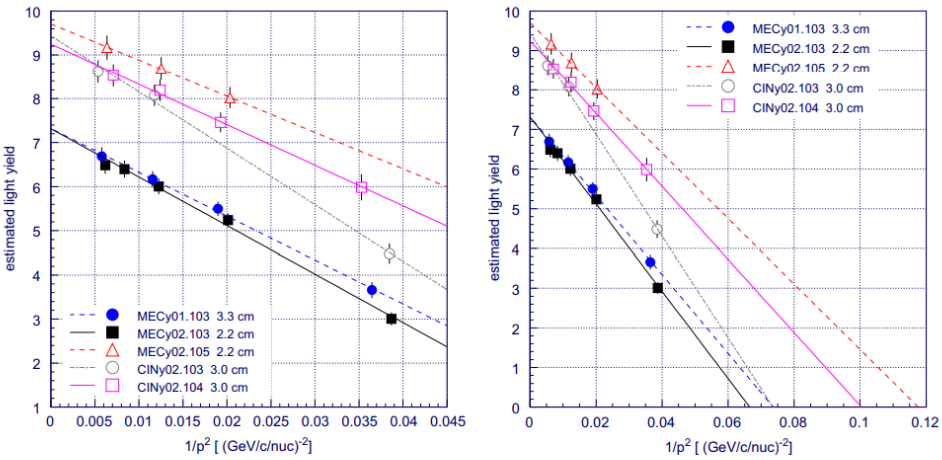

Figure 15: (Left) Evolution of light yield with particle momentum for different aerogel samples, with a fit leaving n as a free parameter. Using $1/p^2$ instead of p makes the fit linear, with the y-axis crossing point corresponding to the light yield estimate. (Right) The same plot with a different scale. The refractive index of each sample is directly determined from the value of $1/p^2$ for which the light yield reaches zero.

flight configurations and for the chosen aerogel (CINy03.105). Therefore, the light guide efficiency obtained in the prototype is on these conditions 60% while the average light guide efficiency expected for the flight is 65%, with a value of 71% for vertical tracks.

There is also a difference between the prototype and flight configuration regarding the supporting plastic foil under the radiator. In the prototype test no foil was used while the flight configuration included a Hesa-Glas foil which is highly transparent for wavelengths above 350nm but becomes increasingly absorbing at lower wavelengths. The loss of photons in the Hesa-Glas foil, dominated by the reflection component, has been estimated to be 8.3% by performing full simulations of the final detector with and without foil. The simulations used photons simulated according to the Cherenkov spectrum, included the radiator interactions (absorption and scattering), light guide absorption and the photomultiplier quantum efficiency.

A correction must also be performed for slight differences in optical properties between the aerogel samples used in the prototype and flight set-ups. The prototype sample had a refractive index $n = 1.0529$ and a clarity $C = 0.0055\mu\text{m}^4\text{cm}^{-1}$ while average values for the tiles used in the final detector are $n = 1.050$ and $C = 0.0061\mu\text{m}^4\text{cm}^{-1}$. The lower refractive index will reduce the light yield obtained at $\beta = 1$ (which is proportional to $1 - 1/n^2$) by 5%, while the increase in Rayleigh scattering due to a higher clarity is estimated to reduce the light collection by a further 4%.

Table 5: List of differences between the RICH prototype and flight detectors.

Item	Prototype	Flight
Matrix layout		
Light guide pitch	31 mm	37 mm
Pixel size	7.75 mm	8.5 mm
Active area	100%	84.4%
Materials		
Radiator foil	None	Hesa-Glas
Light guide foil	Bicron BC-800	Hesa-Glas
Light guide material	Bicron BC-800	Diakon LG-703
Photon collection		
Photon light guide angle	18.7°	0 – 50°
Light guide efficiency	60%	71% (vertical tracks), 65% (average)

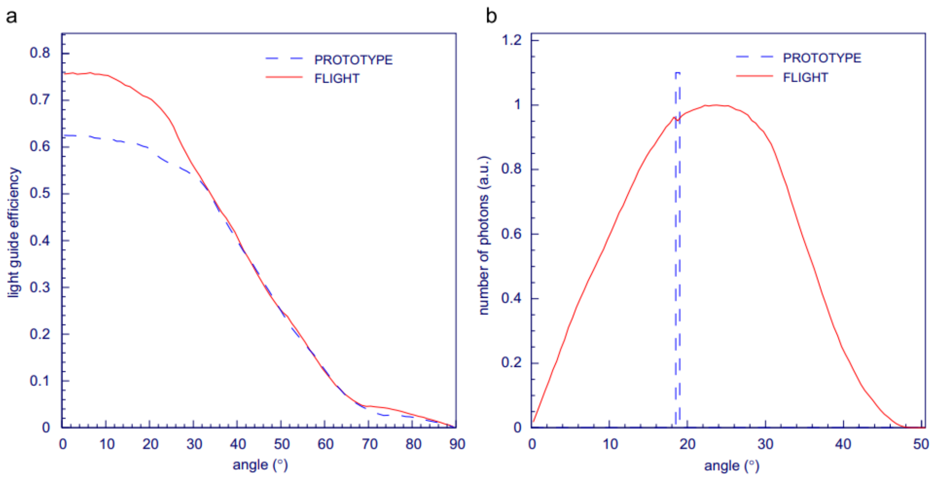

Figure 16: (a) Light guide efficiency as function of photon incidence angles. (b) Distribution of incidence angles with respect to vertical for photons reaching the light guides. The prototype case corresponds to the aerogel sample selected for the flight configuration.

In all data samples considered for the present work the mirror segment was not present and the test beam impacted the RICH detector at a right angle. Therefore, Cherenkov radiation from beam particles always produced circular patterns. AMS-02 events will usually have more complex patterns, with rings having reflected and/or invisible parts. This means that the average ring acceptance will be considerably lower than 100%.

When all differences between the prototype and flight set-ups are considered, the light yield of events with perpendicular incidence for the flight configuration can be calculated using the factors presented in Table 6. The average light yield for a fully contained, non-reflected Cherenkov ring produced by a singly charged particle travelling at $\beta \simeq 1$ and crossing the RICH detector in a trajectory orthogonal to the radiator and detection planes is expected to be around $N_\beta^{(\beta=1)} = 12.2$ photoelectrons. This value, although $\sim 10\%$ higher, is in reasonable agreement with the estimate obtained from simulations of perpendicular events in the AMS-02 detector.

In order to study the light yield dependence with the incidence angle in the detector

Table 6: Estimation of flight light yield (perpendicular incidence) at $\beta = 1$ based on prototype result.

Component	Correction factor
Prototype light yield	14.59 p.e.
Active matrix area	$\times 0.844$
Light guide efficiency	$\times 1.083$
Radiator foil absorption	$\times 0.917$
Aerogel refractive index	$\times 0.95$
Aerogel clarity	$\times 0.96$
Flight estimate	12.2 p.e.

flight configuration, event samples were simulated according to the AMS-02 geometrical acceptance. The expected number of photoelectrons will vary with the particle's incidence angle. The factors contributing to this variation are the light production, the radiator absorption and radiator-air interface effects and the light guide collection efficiency. Fig. 17(a) shows the estimated light yield, normalized to full ring acceptance, as function of the particle polar angle. Particles inciding at higher angles are radiating more photons due to their longer trajectories inside the radiator. Nevertheless, the light yield decreases due to the dominant light guide efficiency factor. This effect is attenuated at larger angles due to the presence of a significative fraction of reflected photons that are collected in the light guides at lower and more efficient angles.

Fig. 17(b) shows the expected distribution of inclinations and acceptances for events in AMS-02. A large fraction of events have polar angles between 20° and 30° and have ring acceptances around 80%.

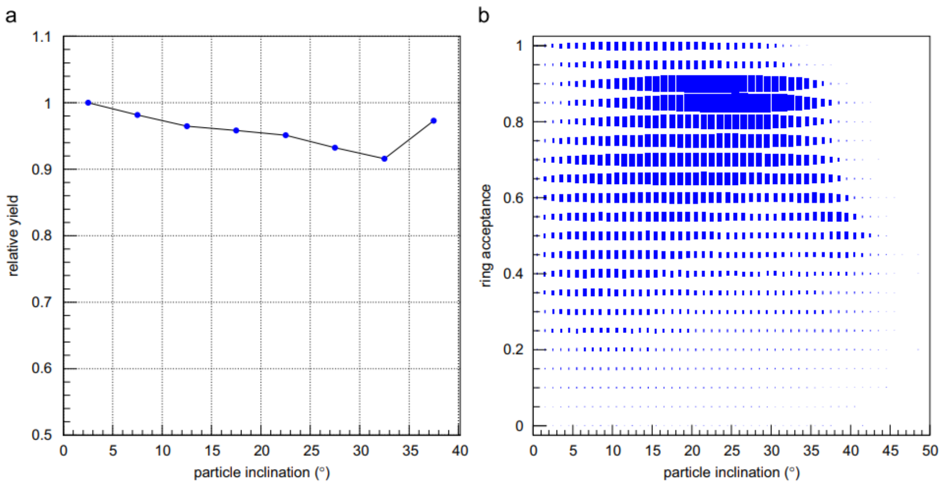

Figure 17: (a) Expected variation of visible light yield (normalized to full ring acceptance) with particle inclination. (b) Expected distribution of particle inclination and visible acceptance for AMS-02 events with $\beta \geq 1$ radiating in aerogel.

A pre-integration of all the detector systems of the AMS-02 spectrometer excepting the superconducting magnet, took place in 2008. A large data sample of cosmic ray events passing within the detector acceptance was gathered in the context of DAQ tests. Based on a very preliminary data analysis, an estimation of the aerogel light yield was derived giving a result $\sim 15\%$ lower than the value expected from simulation which is a positive first indication of the general performance of the system. A future in-beam test to occur at CERN during 2009 will provide more data for a better detector evaluation.

8 Conclusions

Beam tests with the ring imaging Cerenkov detector were performed in 2002 and 2003. Different batches of aerogel samples were tested and light yield evaluated. The analysis of the aerogel samples was performed and a method was developed for the light yield determination. This allowed to make the choice of an aerogel from Boreskov Institute (Novosibirsk), $n = 1.05$ which presented both good optical transparency and high light yield. In test beam conditions, the measured light yield for the selected aerogel was 14.6 photoelectrons, which is in full agreement with the Monte Carlo expectation. The extrapolation of the test beam measurements to the RICH flight set-up configuration gives an estimate of 12.2 photoelectrons for full acceptance rings at perpendicular incidence, a result $\sim 10\%$ higher than AMS-02 simulation estimates.

Acknowledgements

The authors are grateful to the SPS CERN staff for providing the SPS ion beam, and particularly to I. Efthymiopoulos for his constant availability and for his beautiful work in the secondary beam tuning. They are also grateful to the Budker Institute from Novosibirsk (A. Danyliuk, E. Kravchenko, and A. Onuchin), and to the Hamamatsu Company for providing aerogel tests samples, to J. Berger (LPSC) for his help in the CERN run preparation, to Y. Yoshizawa (Hamamatsu Inc.) for technical informations provided to the authors, and to I. Pshenichnov for making his ion fragmentation cross-section calculations available to the authors for the secondary beam study.

References

[1] M. Aguilar, et al. AMS Collaboration, Phys. Rep. 366 (2002) 331.

[2] J. Alcaraz, et al., Nucl. Instr. and Meth. A 478 (2002) 119.

[3] M. Bufnernd, Nucl. Instr. and Meth. A 502 (2003) 158.

[4] M.L. Arruda, Charge and velocity reconstruction with the RICH detector of the AMS experiment—analysis of the RICH prototype data, Ph.D. Thesis, Instituto Superior Técnico, Technical University of Lisbon, January 2008.

[5] P. Aguayo, et al., Nucl. Instr. and Meth. A 560 (2) (2006) 291.

[6] M. Bufnernd, et al., Fragments from the CERN SPS Pb ions as a test beam for the AMS RICH, AMS note, May 2002.

[7] B. Alpat, et al., Nucl. Instr. and Meth. A 540 (1) (2005) 121.

[8] L. Amati, et al., in: Proceedings of the 9th Topical Seminar on Innovative Particle and Radiation Detectors, Nucl. Phys. B (Proc. Suppl.) 150 (2006) 276.

[9] http://panasonic-electric-works.net/.

[10] http://www.catalysis.msk.su/.

[11] F. Barao, et al., Nucl. Instr. and Meth. A 502 (2003) 310.

[12] M.L. Arruda, Cherenkov Ring Acceptance in the RICH Detector of the AMS experiment—optimization of a dual radiator configuration, Master's Thesis, Instituto Superior Técnico, Technical University of Lisbon, June 2003.

[13] E. Lancioni, Estudio de las capacidades del detector RICH de AMS mediante el análisis de los datos de un prototipo en un haz de iones, Ph.D. Thesis, Universidad Complutense de Madrid, 2006.